

AMFD: Distillation via Adaptive Multimodal Fusion for Multispectral Pedestrian Detection

Zizhao Chen, Ye qiang Qian, *Member, IEEE*, Xiaoxiao Yang *Member, IEEE*,
Chunxiang Wang, *Member, IEEE*, and Ming Yang, *Member, IEEE*

Abstract—Multispectral pedestrian detection has been shown to be effective in improving performance within complex illumination scenarios. However, prevalent double-stream networks in multispectral detection employ two separate feature extraction branches for multi-modal data, leading to nearly double the inference time compared to single-stream networks utilizing only one feature extraction branch. This increased inference time has hindered the widespread employment of multispectral pedestrian detection in embedded devices for autonomous systems. To efficiently compress multispectral object detection networks, we propose a novel distillation method, the Adaptive Modal Fusion Distillation (AMFD) framework. Unlike traditional distillation methods, the AMFD framework fully leverages the original modal features from the teacher network, thereby significantly enhancing the performance of the student network. Specifically, a Modal Extraction Alignment (MEA) module is utilized to derive learning weights for student networks, integrating focal and global attention mechanisms. This methodology enables the student network to acquire optimal fusion strategies independent from that of teacher network without necessitating an additional feature fusion module. Furthermore, we present the SMOD dataset, a well-aligned challenging multispectral dataset for detection. Extensive experiments on the challenging KAIST, LLVIP and SMOD datasets are conducted to validate the effectiveness of AMFD. The results demonstrate that our method outperforms existing state-of-the-art methods in both reducing log-average Miss Rate and improving mean Average Precision. The code is available at <https://github.com/bigD233/AMFD.git>.

Index Terms—Pedestrian Detection, Knowledge Distillation, Multimodal Fusion

I. INTRODUCTION

Pedestrian detection is a crucial problem in computer vision, with applications ranging from autonomous vehicles [1] to surveillance systems [2]. Modern studies using visible images perform well under regular light conditions. However, due to susceptibility to lighting conditions, visible light exhibits poor detection performance in complex low-light scenarios. To mitigate this limitation, thermal infrared images are introduced to provide supplementary data, leading to the exploration of multispectral pedestrian detection [3] as a potent solution.

This work is supported by the National Natural Science Foundation of China under Grant 62103261. (Corresponding author: Ye qiang Qian; Ming Yang.)

Zizhao Chen, Ye qiang Qian, Xiaoxiao Yang, Chunxiang Wang and Ming Yang are with the Department of Automation, Shanghai Jiao Tong University, Key Laboratory of System Control and Information Processing, Ministry of Education of China, Shanghai, 200240, China (email: qianye-qiang@sjtu.edu.cn; mingyang@sjtu.edu.cn).

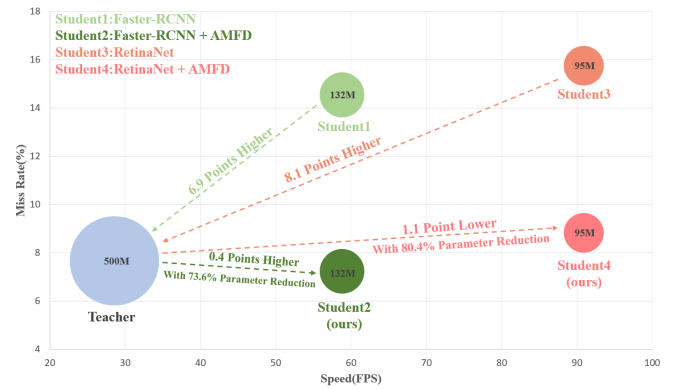


Fig. 1. The experimental results of pedestrian detection on KAIST [3] dataset. The teacher is a two-stream network with a complex fusion module and ResNet50 backbone [4]. The students are single-stream networks (Faster-RCNN [5] and RetinaNet [6]) with simple image-level fusion and ResNet18 backbone [4].

Multi-modal feature fusion is the key to multispectral detection. Previous works [7]–[14] have explored various fusion strategies: early, mid, and late fusion. In the mid-fusion framework, thermal and RGB features are extracted independently and subsequently fused at the intermediate stage of the two-stream network. Recent research employing the mid-fusion strategy has shown superior performance in multispectral detection. Nevertheless, the adoption of mid-fusion strategies in two-stream networks incurs significant computational overhead, while nearly doubling the inference speed compared to single-stream networks, thereby posing challenges for deployment on embedded devices [15].

In efforts to minimize inference time, many researchers focus on model compression through knowledge distillation, a technique aimed at transferring information from a large teacher network to a compact student network, thereby reducing model inference time. Recently, many feature-based knowledge distillation methods [16]–[19] have been proposed for the field of multispectral object detection. However, these methods face a challenge in transferring the knowledge of the fusion feature from specific modules of the teacher network to the student network. Since complex feature fusion modules are often present in teacher networks but not in simple student networks, this increases the capacity gap [20], [21] between teacher and student networks. Moreover, direct distillation of the fusion features ignores much potentially useful information

arXiv:2405.12944v1 [cs.CV] 21 May 2024

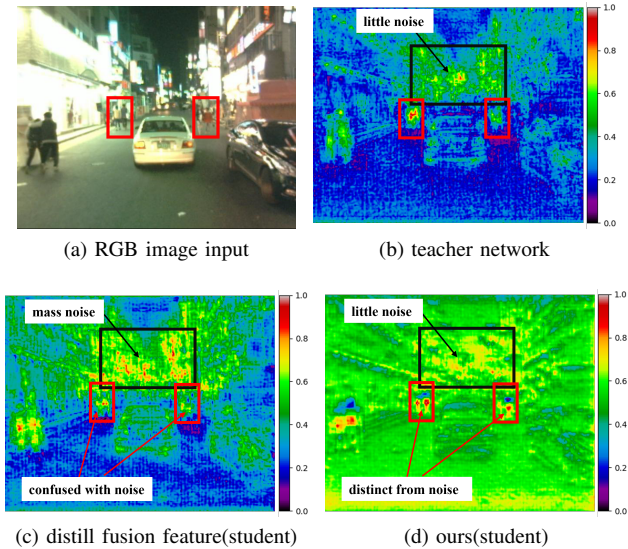


Fig. 2. Based on the fusion feature maps of different networks, we obtain the spatial attention of the feature map. We can see that (c) is similar to (b), but the noise in the black box is not suppressed. Noise makes pedestrians in the two red boxes in figure (a) not easily recognizable in figure (c). Our method shown in (d) no longer follows the fusion strategy of teacher can well represent the pedestrian features.

in the original modal features of the teacher network. As a result, the student network struggles to effectively assimilate the fusion strategy of the teacher network. As shown in Fig.2c, directly learning the fusion features of the teacher network will introduce more noise into the student network, indicating that the fusion strategy suitable for the teacher network may not necessarily be suitable for the small-capacity student network.

To address the above issues, we propose an Adaptive Modal Fusion Distillation framework (AMFD). Specifically, a fusion distillation architecture is introduced. Instead of directly distilling fusion features from the teacher network to the student network, we simultaneously distill the thermal and RGB features of the teacher network to the fusion features of the student network. This approach aims to enable the student network to develop its own efficient fusion strategy during training. Drawing inspiration from GcBlock [22], we design the modal extraction alignment (MEA) module, which obtains distillation losses based on focal and global attention mechanisms. The fusion features of the student network are learned from thermal and RGB features through distillation losses calculated by the MEA module. This approach liberates the student network from the constraints of the teacher network and significantly enhances the performance of the student network.

In summary, our contributions are as follows.

- We innovatively propose the Adaptive Modal Fusion Distillation method, which front-loads the distillation location through the fusion distillation architecture. Two Modal Extraction Alignment (MEA) modules are also used to extract infrared and visible modal features, respectively, so that the student network can efficiently generate fusion strategies independent of the instructor network, thus efficiently compressing the teacher network to a compact student network, which

reduces the inference speed.

- We present the SJTU Multispectral Object Detection (SMOD) dataset for detection. Within this dataset, 8042 pedestrians, 10478 riders, 6501 bicycles, and 6422 cars are annotated. The degree of occlusion of all objects is meticulously annotated. The dataset with low sampling rate has dense rider and pedestrian objects and contains rich illumination variations in its 3298 pairs of images of night scenarios. Our dataset is available on Kaggle¹.

- The experiments on KAIST [3], LLVIP [23] and our SMOD datasets show that student networks can achieve excellent distillation results without adding additional modules. Our AMFD distillation method on the KAIST [3] dataset can reduce the log-average miss rate (MR^{-2}) of the student network to 0.4% lower than that of the teacher network, while the inference time is reduced to half of that of the teacher network. On the LLVIP [23] dataset, our method improves the COCO Mean Average Precision (mAP) of the student network by 2.7%. On the SMOD dataset, we validate the effectiveness and flexibility of the fusion distillation architecture.

II. RELATED WORK

A. Multispectral Pedestrian Detection

Multispectral pedestrian detection, which combines RGB and thermal images, has attracted considerable attention for its ability to maintain robust detection performance under varying lighting conditions. Recent research has concentrated on refining multispectral feature fusion techniques. Zhou et al. proposed MBNet [24] to mitigate the imbalance between different modalities. GAFF [8], introduced by Zhang et al., integrates multispectral features using both inter- and intra-modality attention mechanisms. BAANet [10] leverages modality correlation to recalibrate attention mechanisms for two modalities. MSDS-RCNN [25] enhances pedestrian detection performance by simultaneously conducting pedestrian detection and segmentation. DCMNet [26] focuses on learning both local and non-local information within multispectral features. Some studies employing late fusion strategies have also demonstrated remarkable performance. For example, ProbEn [9] explores late fusion of single-modal detections through detector ensembling. However, these methods primarily rely on two-stream networks with various additional modules, inevitably increasing the inference time and posing challenges for deployment on embedded devices.

B. Knowledge Distillation

Knowledge distillation (KD), pioneered by Hinton et al. [27], is a crucial technique for model compression while preserving network architecture. FitNet [28] and Zagoruyko et al. [29] have, respectively, highlighted the role of intermediate layer semantics and the use of unsupervised attention maps in guiding student models. KD's applications extend beyond image classification to object detection. For example, Wang et al. [30] introduced fine-grained masking to distill regions

¹<https://www.kaggle.com/datasets/zizhaochen6/sjtu-multispectral-object-detection-smod-dataset>

TABLE I
COMPARISON OF SMOD AND EXISTING DATASETS INCLUDING FLIR THERMAL DATASET, CVC-14, KAIST MULTISPECTRAL DATASET, LLVIP DATASET AND M³FD DATASET. THE "PERSON DENSITY" REFERS TO THE NUMBER OF PEDESTRIANS AND CYCLISTS HIGHER THAN 35 PIXELS PER IMAGE.

Dataset	Img Pairs	Sampling Rate	Year	Camera angle	Aligned	Occlusion	Person Density	Bicycle Density
LLVIP	16836	1FPS	2021	surveillance	✓	✗	2.51	✗
M ³ FD	4200	-	2022	multiplication	✓	✗	1.22	0.11
KAIST	95328	20FPS	2015	driving	✓	✓	0.62	✗
CVC-14	8518	10FPS	2016	driving	✗	✗	0.80	✗
FLIR	10228	30FPS	2018	driving	✗	✗	1.52	0.43
SMOD	8676	2.5FPS	2024	driving	✓	✓	2.14	0.79

delineated by ground-truth bounding boxes, while Guo et al. [31] highlighted the significance of distilling both foreground and background information separately, leading to improved student performance.

For multispectral detection, Liu et al. [18] proposed a method that employs distinct distillation losses at multiple levels, encompassing the perspective of feature, detection, and segmentation. Zhang et al. [19] designed a knowledge transfer module to transfer knowledge from the fusion features extracted by GAFF [8] of the teacher network. However, these methods often rely on teacher network fusion features and additional student network modules, contrary to the goal of minimizing inference time. Our framework diverges by distilling original modal features, enabling robust student network performance without added inference latency.

C. Multispectral Pedestrian Dataset

In recent years, many multispectral pedestrian detection datasets have been proposed. Both CVC-14 [32] and FLIR are multispectral datasets proposed for automated driving pedestrian detection tasks. However, the visible and infrared image pairs in these two datasets are not well aligned spatially and temporally. The KAIST [3] dataset provides well-aligned picture pairs, annotated pedestrian occlusions, and is now widely used for multispectral pedestrian detection tasks. However, its original data sampling rate is too high, resulting in little variation in consecutive frame images, thus requiring data cleaning when in use. In addition to the above dataset in driving angle, LLVIP is a well-aligned multispectral dataset in surveillance angle. Most of the images in the LLVIP dataset are collected from a medium distance, so the dataset lacks small-target pedestrian. The M³FD dataset [33] covers four major scenarios with various environments, having a wide range of pixel variations. Since some of these scenarios are not driving scenarios, such as in the woods and on grass, the authors call it a "multiplication" angle. However, this also results in a low number of pedestrians in the data.

In addition to this, we find that the density of "effective" person (defined as pedestrians with a height higher than 35 pixels) in the dataset in the driving view are all relatively low. Tab.I shows the details of these datasets and our proposed SMOD dataset. In order to avoid the above disadvantages of existing datasets, we propose the SMOD dataset. We compare the effective pedestrian density (the average number of "effective" person per image) in these datasets in Tab.I

to characterize the abundance of pedestrians included in the dataset captured in our campus scene.

III. METHOD

A. Overall Architecture

As shown in Fig.3, the two-stream teacher network has two feature extractors, which contains the backbone and feature pyramid networks (FPN) [34]. Then the feature fusion module of the teacher network generates the fusion feature for the following detection. The teacher network is recognized as having excellent feature extractor and fusion feature. In contrast, the student network has only one feature extractor with a smaller backbone compared to the teacher network. The input of the backbone is the fusion of RGB and thermal infrared (TIR) images. Notably, the single stream with simple image-level fusion input has been shown to perform poorly in multispectral pedestrian detection. Hence, our objective is to enhance the performance of student networks with small capacity.

The distillation via Adaptive Modal Fusion (AMFD) focuses on the RGB and TIR features. To exploiting potentially useful information in original modal features and efficiently guide the student network in formulating a fusion strategy, we leverage a fusion distillation architecture. This approach involves distilling multi-modal feature knowledge from the teacher network into the fusion feature of the student network. The Modal Extraction Alignment (MEA) module aligns the feature maps using global and focal attention mechanisms. These MEA modules dynamically generate channel-wise weights to learn the useful part of the RGB and TIR features. Then the student network is optimized by the MEA losses and the original detection loss. Consequently, student networks can generate more suitable fusion strategies independently of teacher networks.

B. Fusion Distillation Architecture

Feature-based knowledge distillation aims to enable student networks to learn and mimic the mid-level features of teacher networks. Routinely, traditional methods select features at the same stage for distillation. That is, the student network will mimic the features generated by identical modules of the teacher network during the distillation process. Thus, distilling the fusion features of the teacher network to the fusion features of the student network naturally becomes the

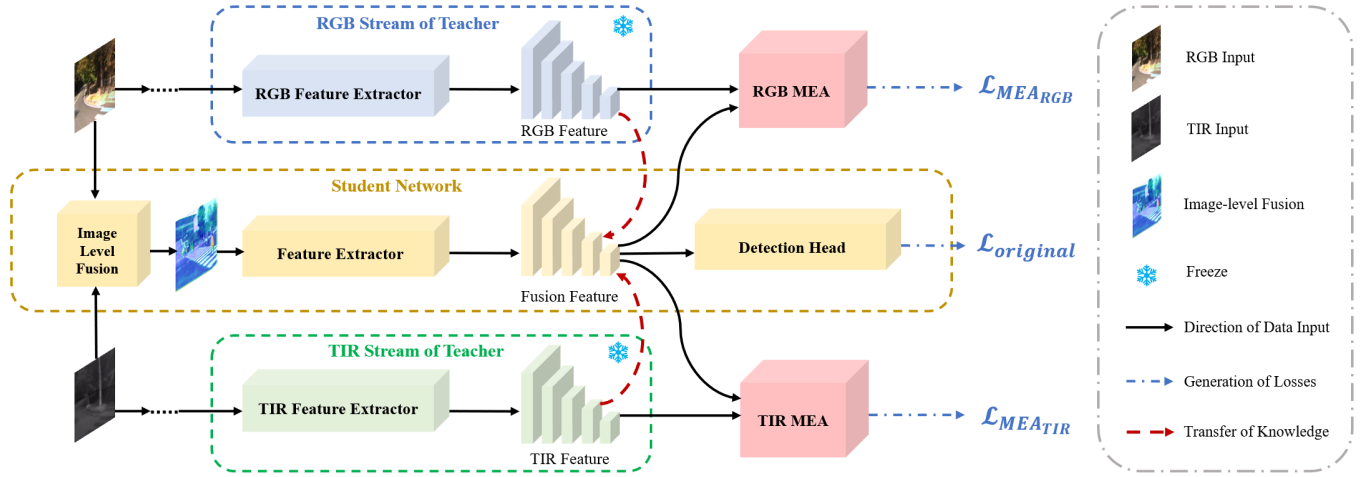


Fig. 3. The overall architecture of the proposed distillation framework. Firstly, we use a frozen two-stream network with complex feature extractor as the teacher network. The student network is a single-stream network with a simple image-level fusion module. Then during training, the framework distills the knowledge of RGB and TIR features of the teacher network into the fusion features of the student network through the fusion distillation architecture. The fusion distillation architecture contains two modal extraction alignment modules (MEA) to adaptively extract the difference between the fusion feature of the student network and the RGB, TIR feature of the teacher network. At last, the student network is optimized by two MEA losses produced by MEA and the original detection loss.

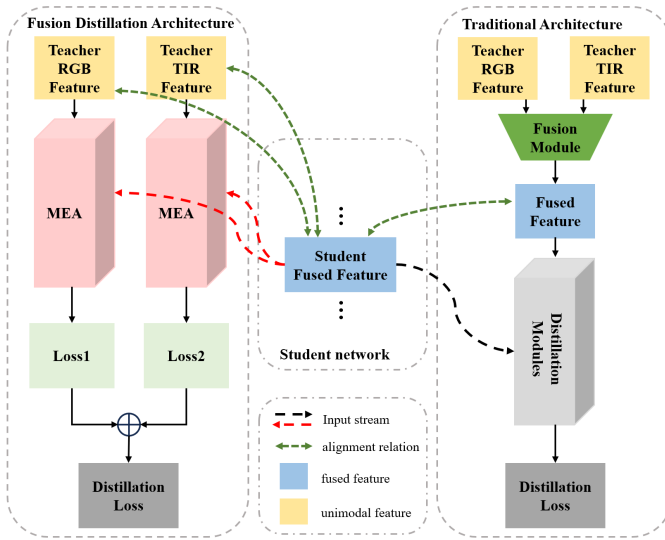


Fig. 4. The comparison between fusion distillation architectures and traditional architecture. The position of the feature for distillation is advanced from the fusion feature to the original modal feature.

dominant distillation architecture. Based on this architecture, many approaches [18], [19] will add some specific modules to the single-stream student network to improve distillation results. However, this situation limits the structure of the student network and also increases the complexity of the student network, which is not conducive to its deployment.

To maintain the flexibility of the student network structure while enabling it to generate efficient feature fusion strategies, we propose a fusion distillation architecture. As shown in Fig.4, the fusion features of the student network are simultaneously aligned to TIR and RGB features of the teacher network. We denote the RGB feature and the TIR feature, which is the output of its feature pyramid network(FPN [34]) as x_R and

x_T . The $\mathcal{F}(\cdot)$ denotes feature fusion module while the $\mathcal{L}(\cdot)$ denotes the loss function of the distillation. The distillation loss of the traditional architecture is defined as

$$L_{traditional} = \mathcal{L}(\mathcal{F}(x_R, x_T), \tilde{x}_F), \quad (1)$$

where the \tilde{x}_F is the fusion feature of the student network. While the fusion distillation architecture no longer relies on the feature fusion module of the teacher network. The distillation loss of the fusion distillation architecture is:

$$L_{fusion} = \mathcal{L}(x_R, \tilde{x}_F) + \mathcal{L}(x_T, \tilde{x}_F). \quad (2)$$

This loss indicates that during distillation, the fusion features of the student network must emulate both the TIR and RGB features. In contrast to the distillation loss of the traditional architecture, this loss will not lose potentially useful information during feature fusion. Consequently, the student network can fully leverage unfused modal features to devise fusion strategies independent of those of the teacher networks.

C. Modal Extraction Alignment Module (MEA)

Designing an effective distillation loss is a key issue in the field of object detection distillation. The extreme imbalance between the foreground and the background is a key issue in the field of object detection [6] and distillation. To address this issue, we extract the global and focal knowledge separately. As shown in Fig.5, the modal extraction alignment module (MEA) consists of two parts: Global Feature Extraction and Focal Feature Extraction. In the following subsection we will introduce these two modules, respectively.

1) **Global Feature Extraction:** Global information distillation is the most direct and efficient distillation method. This permits maximum retaining of global information and also allows more globally relevant dark knowledge to be transferred from the teacher network to the student network. However, the

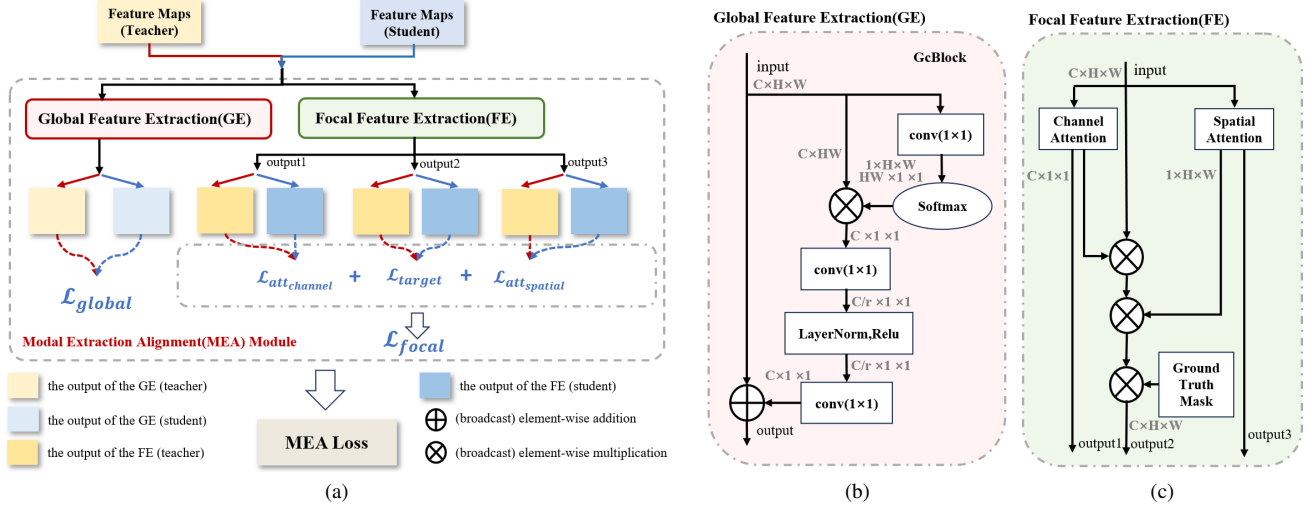


Fig. 5. The structure of our modal extraction alignment (MEA) module. (a) shows the overall structure of the MEA module. Both input features go through two modules, Global Feature Extraction (GE) and Focal Feature Extraction (FE), which ultimately form a MEA loss consisting of the global loss and focal loss. (b) and (c) show the details of the GE and FE. GE generates a $C \times 1 \times 1$ weight and this weight is added to the original feature map by broadcast channel-wise addition, aiming to obtain a feature map with better global relation.

features of the student network have to be aligned with the features of multiple modalities at the same time because of the fusion distillation architecture. This requires us to pay attention to different information according to different modalities in the global distillation. Hence, it is important to merge different information in the global distillation corresponding to different modalities.

To enhance the extraction of global relations, we use GcBlock [22] to ensure that the student network possesses the same global relations as the teacher network. The GcBlock here is to extract important global relations in different modalities and make the student network adaptively learn these relations. The GcBlock will generate a channel-wise weight:

$$\mathcal{W}(x) = \mathcal{F}_{conv3}(\mathcal{LR}(\mathcal{F}_{conv2}(\sum_{j=1}^{N_p} \frac{e^{\mathcal{F}_{conv1}(x_j)}}{\sum_{m=1}^{N_p} e^{\mathcal{F}_{conv1}(x_m)}} x_j))). \quad (3)$$

And add this weight to the input feature map, then we get the output feature map with global relations:

$$\mathcal{G}(x) = x \oplus \mathcal{W}(x), \quad (4)$$

where \mathcal{F}_{conv} denotes the 1×1 convolution layers, \mathcal{LR} denotes the layer normalization and relu activation. N_p is the number of pixels of the feature x , and x_j, x_m is the slice of the feature map ($C \times 1 \times 1$, C is the number of channels in the feature map). \oplus denotes the broadcast element-wise addition.

So for the RGB, TIR feature maps x_R, x_T of teacher network and the fusion feature \tilde{x}_F of the student network, the global feature extraction loss is:

$$\mathcal{L}_{global_{TIR}} = \lambda_1 \sum (\mathcal{G}_1(x_T) - \mathcal{G}_1(\tilde{x}_F))^2, \quad (5)$$

$$\mathcal{L}_{global_{RGB}} = \lambda_2 \sum (\mathcal{G}_2(x_R) - \mathcal{G}_2(\tilde{x}_F))^2, \quad (6)$$

$$\mathcal{L}_{global} = \mathcal{L}_{global_{TIR}} + \mathcal{L}_{global_{RGB}}, \quad (7)$$

where $\mathcal{G}_1, \mathcal{G}_2$ are the GcBlocks in two MEA modules used to distill the TIR and RGB feature of the teacher network

respectively. λ_1 and λ_2 are hyper-parameters to balance the loss.

2) **Focal Feature Extraction:** Focusing solely on global relations is obviously insufficient. The global distillation process carries the risk of introducing noise, which could adversely affect the features of the target area. To enable the student network to acquire more precise knowledge about the features of the target area, we emphasize crucial pixels and attention maps in the feature map. Building upon this, we introduce focal feature extraction.

Obviously the areas we focus on are areas where pedestrians are present. So we select the area based on the ground-truth bounding boxes. These areas are marked by a mask M :

$$M_{i,j} = \begin{cases} \frac{1}{h_b w_b} & , \text{if } (i, j) \in b \\ 0 & , \text{Otherwise} \end{cases}, \quad (8)$$

where the b denotes the ground-truth boxes corresponding to the feature map scale, h_b, w_b are the height and width of the ground-truth box with the largest area that this pixel belongs to. The weight $\frac{1}{h_b w_b}$ balances the composition of the losses. This way, the losses generated for targets with larger areas do not account for the majority of the losses.

The mask M selects the regions that are important to us. However, the weights for the areas within a ground-truth box are uniform both spatially and across channels. Inspired by the attention mechanism, we will calculate the focal feature loss according to the channel and spatial attention map. This involves calculating the absolute mean values on both pixel and channel dimensions, followed by generating weights using softmax.

$$A^S(x) = H \cdot W \cdot \text{softmax}\left(\frac{1}{C} \sum_{c=1}^C |x_c|\right), \quad (9)$$

$$A^C(x) = C \cdot \text{softmax}\left(\frac{1}{HW} \sum_{i=1}^H \sum_{j=1}^W |x_{i,j}|\right), \quad (10)$$

where the $A^S(x)$, $A^C(x)$ are the spatial and channel attention maps of the feature x . Then the loss after spatial, channel attention and mask weighting of target area is:

$$\mathcal{L}_{target_{RGB}} = \alpha_1 \sum_{k=1}^C \sum_{i=1}^H \sum_{j=1}^W M_{i,j} A_{i,j}^{S_R} A_k^{C_R} (x_R - \tilde{x}_F)^2, \quad (11)$$

$$\mathcal{L}_{target_{TIR}} = \alpha_2 \sum_{k=1}^C \sum_{i=1}^H \sum_{j=1}^W M_{i,j} A_{i,j}^{S_T} A_k^{C_T} (x_T - \tilde{x}_F)^2, \quad (12)$$

where α_1 and α_2 are hyper-parameters to balance the loss. Note that A^{S_R} , A^{C_R} and A^{S_T} , A^{C_T} are the spatial and channel attention for RGB and TIR feature of the teacher network, respectively.

Although we obtain the loss of important regions using spatial and channel attention of the teacher network, we do not constrain spatial and channel attention of the student network. In order for the student network to learn spatial attention and channel attention of the two modalities of the teacher network in an integrated manner, we design the attention loss:

$$\mathcal{L}_{att_{RGB}} = \gamma_1 (l(A^{S_R}, A^{S_F}) + l(A^{C_R}, A^{C_F})), \quad (13)$$

$$\mathcal{L}_{att_{TIR}} = \gamma_2 (l(A^{S_T}, A^{S_F}) + l(A^{C_T}, A^{C_F})), \quad (14)$$

where γ_1, γ_2 are hyper-parameters to balance the loss, and l denotes the L1 loss. In this way, the spatial and channel attention A^{S_F}, A^{C_F} of the student network can learn from teacher network and generate fusion attention that is suitable for itself. Then the loss generated by the focal feature extraction is:

$$\begin{aligned} \mathcal{L}_{focal} &= \mathcal{L}_{focal_{RGB}} + \mathcal{L}_{focal_{TIR}} \\ &= \mathcal{L}_{target_{RGB}} + \mathcal{L}_{att_{RGB}} + \mathcal{L}_{att_{TIR}} + \mathcal{L}_{target_{TIR}}. \end{aligned} \quad (15)$$

3) **Total MEA Loss:** The total loss is generated by two MEA modules. The two MEA modules transfer the knowledge of the RGB feature and the TIR feature from the teacher network to the student network. The student network generates the fusion strategy during training optimized by the MEA loss:

$$\begin{aligned} \mathcal{L}_{MEA} &= \mathcal{L}_{MEA_{RGB}} + \mathcal{L}_{MEA_{TIR}} \\ &= \mathcal{L}_{global_{RGB}} + \mathcal{L}_{focal_{RGB}} + \mathcal{L}_{global_{TIR}} + \mathcal{L}_{focal_{TIR}}. \end{aligned} \quad (16)$$

D. Overall Loss

The total loss of the adaptive modal fusion distillation is:

$$\mathcal{L} = \mathcal{L}_{original} + \mathcal{L}_{MEA}, \quad (17)$$

where $\mathcal{L}_{original}$ is the original detection loss of the detector. Our frame work only need the feature after the FPN of the

teacher network. So, the framework can be used in many types of detectors.

IV. SMOD DATASET

We propose the SJTU Multispectral Object Detection (SMOD) Dataset for detection.

A. Image Capture and Registration

The images are captured by the Asens FV6, a binocular vehicle camera platform that consist of a visible light camera and a infrared camera. Due to the different field of view of different sensor cameras, we clip and register visible images to make image pairs strictly aligned. Fig.6 shows the different field sizes of different cameras and the visible image after registration. We also provide unregistered image pairs and annotations for researchers to study visible and infrared image registration. The dataset contains 5378 pairs of images of daytime scenes taken at 3pm and 3298 pairs of images of nighttime scenes taken at 7pm.



(a) different field of views

(b) clipped visible images

Fig. 6. Image capture and image registration. The visible light camera and the infrared camera has the different field of views shown in (a). The image pairs are aligned after clipped and registered the visible images shown in (b).

B. Annotations and Advantages

We annotate four categories of targets: pedestrians, riders, cars, and bicycles. In particular, we annotate the degree of occlusion for each type of object. As shown in Tab.II, we categorize occlusion into four categories based on the percentage of occlusion: no occlusion (NO), light occlusion (LO), moderate occlusion (MO), and heavy occlusion (HO).

TABLE II
NUMBER OF EACH TYPE OF OBJECT IN THE SMOD DATASET WITH DIFFERENT DEGREES OF OCCLUSION. THE "O" DENOTES THE PERCENTAGE OF THE OBJECT THAT IS OCCLUDED.

Object	NO	LO	MO	HO
	$O = 0\%$	$O < 30\%$	$30\% \leq O < 60\%$	$60\% \leq O < 90\%$
pedestrian	4007	1902	1285	848
rider	8151	1024	721	582
bicycle	3039	1852	1762	1279
car	1819	1118	1595	1890

Tab.I shows the comparison of SMOD and the existing datasets mentioned in Section 2. Our SMOD dataset has the following advantages:

- Since the image pairs are taken on campus, the majority of image pairs contain very abundant and dense objects, especially bicycle and perosn. This shows that this is a challenging dataset for multispectral object detection.

- The images of the dataset are sampled at a frequency of 2.5 FPS, which is substantially lower compared to other multispectral pedestrian detection datasets for driving scenarios, which avoids the process of neighboring frames being too similar to each other and subsequent cleaning of the dataset by the user.

- Visible-infrared images are aligned strictly in time and space and we annotate three other types of objects which are common in driving. Thus, image pairs can be used for other driving scene tasks other than object detection, such as image fusion and supervised image-to-image translation.

- The image pairs in our dataset contain rich illumination variations, particularly at night, such as the very low illumination and strong light shown in Fig.7. Therefore, the dataset is suitable for the study of image fusion and low-light pedestrian detection for driving.



Fig. 7. Image pairs in the SMOD dataset with rich objects and strong light.

V. EXPERIMENTS

A. Dataset and Evaluation Metric

KAIST: KAIST dataset [3] is a widely used benchmark dataset in multispectral pedestrian detection. Since the original annotation of the dataset contains noise, we use the improved annotation proposed by [35] and the sanitized annotation proposed by [25] for training. The test annotation we adopt is improved by [36]. The log-average Miss Rate (MR^{-2}) is calculated by averaging the False Positive Per Image (FPPI) sampled within the range of $[10^{-2}, 10^0]$, the lower the better. We adopt the MR^{-2} as our evaluation metric under the "reasonable" settings (excluding pedestrians that are occluded or shorter than 55 pixels).

LLVIP: LLVIP dataset [23] is a challenging dataset for multispectral pedestrian detection including 12,025 training images and 3,463 test images. We use the COCO-style Average Precision [37] as evaluation metrics.

SMOD: We introduce this dataset in detail in Section.4. We divide 1876 pairs of images from a total of 8676 pairs as the test set, which contains 1178 pairs of daytime images and 698 pairs of nighttime images. We use both the COCO-style

Average Precision [37] as evaluation metrics and log-average Miss Rate (MR^{-2}) mentioned before.

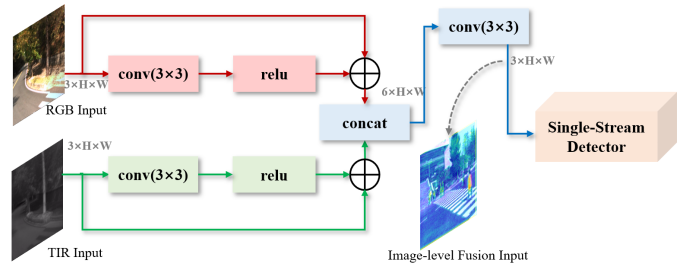


Fig. 8. The structure of image-level fusion. It contains two residual modules and a concatenation module to get simple fusion results as the input.

B. Implementation Details

Network Architecture. We use MMDetection [38], a popular object detection toolkit based on PyTorch [39], to implement our approach. For the teacher network in all experiments, we adopt Faster-RCNN [5] with two ResNet50 backbones [4] and feature pyramid networks [34] (FPN) to extract the RGB and TIR feature, respectively. The teacher network fuse the feature with the cross-modality attention transformer [40]. For the student network, to validate the flexibility of our method, we adopt the popular two-stage detector Faster-RCNN and the one-stage detector RetinaNet [6] with only one ResNet18 [4] and FPN. The fusion of student network is early image-level fusion by the fusion module shown in Fig.8.

Training Details All networks are trained on a single Nvidia GeForce GTX 1080Ti GPU. The batch size is set to be 2 for training. The backbone networks for all experiments are pre-trained on the ImageNet dataset [41]. For all datasets, the learning rate is set to be 1×10^{-4} with the 1×10^{-4} weight decay AdamW optimizer. We train the network for a total of 30,000 iterations. We adopt the hyper-parameters $\{\alpha_1 = \alpha_2 = 5 \times 10^{-5}, \gamma_1 = \gamma_2 = 5 \times 10^{-5}, \lambda_1 = \lambda_2 = 5 \times 10^{-7}\}$ for Faster-RCNN and $\{\alpha_1 = \alpha_2 = 1 \times 10^{-3}, \gamma_1 = \gamma_2 = 1 \times 10^{-3}, \lambda_1 = \lambda_2 = 5 \times 10^{-6}\}$ for RetinaNet.

C. Distillation on KAIST Dataset

TABLE III
THE DISTILLATION RESULTS OF AMFD ON KAIST TRAINED BY THE IMPROVED ANNOTATIONS [35].

Detectors	All	Day	Night	Time
Faster-RCNN(Tea.)	7.66	9.34	5.14	0.12s
<i>trained with the improved annotation</i>				
Faster-RCNN(Stu.)	11.86	14.46	7.02	0.05s
AMFD+Faster-RCNN(Stu.)	7.23	9.83	2.18	
RetinaNet(Stu.)	13.80	15.43	9.99	
AMFD+RetinaNet(Stu.)	8.82	10.98	4.86	0.04s
<i>trained with the sanitized annotation</i>				
Faster-RCNN(Stu.)	14.54	18.99	6.90	0.05s
AMFD+Faster-RCNN(Stu.)	6.65	9.07	2.11	
RetinaNet(Stu.)	12.99	15.67	7.50	
AMFD+RetinaNet(Stu.)	7.66	10.30	3.16	0.04s

TABLE IV
COMPARISON OF THE STUDENT NETWORK DISTILLED BY THE PROPOSED AMFD WITH THE STATE-OF-THE-ART METHODS IN TERMS OF THE LOG-AVERAGE MISS-RATE ON THE KAIST TEST SET.

Methods	Backbone	GPU	All	Day	Night	Time
IAF-RCNN [42]	VGG16	Titan X	15.73	14.55	18.26	0.21
CIAN [43]	VGG16	1080Ti	14.12	14.77	11.13	0.07
AR-CNN [35]	VGG16	1080Ti	9.34	9.94	8.38	0.12
MBNet [24]	ResNet50	1080Ti	8.13	8.28	7.86	0.07
BAANet [10]	ResNet50	1080Ti	7.92	8.37	6.98	0.07
UFF+UCG [44]	ResNet50	1080Ti	7.89	8.18	6.96	0.09
AAANet-RetinaNet [11]	ResNet50	1080Ti	7.51	7.74	7.39	0.06
AAANet-Faster RCNN [11]	ResNet50	1080Ti	6.91	6.66	7.31	0.10
AMFD-Faster RCNN(ours)	ResNet18	1080Ti	7.23	9.83	2.18	0.05
AMFD-RetinaNet(ours)	ResNet18	1080Ti	8.82	10.98	4.86	0.04

Analysis of distillation results. We fix the teacher network to the two-stream Faster-RCNN network described above and trained it using the improved annotation in all distillation experiments. According to the experimental results in Tab.III, AMFD can reduce MR^{-2} of the student network on the All set by a factor of nearly two. When trained with the improved annotations, the inference time of the two-stage student network is reduced by 58.3%, with even 0.4% decrease in MR^{-2} ; meanwhile, the inference time of the one-stage student network is reduced by 66.7% with only 2% higher MR^{-2} . In particular, we find that the student network distilled by AMFD has a low MR^{-2} on the **Night** set, i.e., the network distilled by AMFD has excellent extraction of TIR features. Student networks trained with the sanitized annotation even have better performance than those trained with the improved annotation.

TABLE V
ABLATION STUDY OF THE PROPOSED FUSION DISTILLATION ARCHITECTURE. THE "RGB", "TIR" AND "FUSION" DENOTE WHETHER DISTILL THE RGB, TIR AND FUSION FEATURE RESPECTIVELY.

Detector	RGB	TIR	Fusion	All	Day	Night
Faster-RCNN				11.86	14.46	7.02
			✓	11.03	14.07	5.64
	✓	✓		7.23	9.83	2.18
RetinaNet				13.80	15.43	9.99
			✓	10.93	13.65	5.76
	✓	✓		8.82	10.98	4.86

TABLE VI
ABLATION STUDY OF THE PROPOSED MEA. THE "GLOBAL" AND "FOCAL" DENOTE THE GLOBAL FEATURE EXTRACTION AND FOCAL FEATURE EXTRACTION IN MEA.

Detector	Global	Focal	All	Day	Night
Faster-RCNN			11.86	14.46	7.02
		✓	9.85	13.35	3.24
	✓	✓	7.51	10.12	3.25
RetinaNet			7.23	9.83	2.18
		✓	13.80	15.43	9.99
	✓	✓	11.34	13.97	6.37
	✓		9.62	11.87	5.28
	✓	✓	8.82	10.98	4.86

Ablation experiments and analysis. Ablation experiments are

conducted on the KAIST dataset to demonstrate the effectiveness of the proposed fusion distillation architecture and MEA module. In Tab.V, distilling both the RGB and the TIR features denotes the fusion architecture, and only distilling the fusion features denotes the traditional architecture. For a fair comparison, the distillation modules we use in traditional architecture is also MEA module. The results of the experiment in Tab.V show that the fusion architecture can greatly improve the performance of the student network. In Tab.VI, the "Global" and "Focal" denote global feature extraction and focal feature extraction in MEA. We can find that combining both local and global features is the more effective distillation method. Results of the ablation study demonstrate the effectiveness of the proposed distillation framework.

TABLE VII
COMPARISON OF THE TEACHER AND STUDENT NETWORK WITH OTHER MULTISPECTRAL DISTILLATION METHODS IN TERMS OF THE LOG-AVERAGE MISS-RATE ON THE KAIST TEST SET

Detector	Distill	MR(All)	Time
DCRL [18] (Tea.)	-	9.16	0.175s
DCRD [18] (Stu.)	✓	12.58	0.128s
MD [19] (Tea.)	-	7.77	11ms
MD [19] (Stu.)		9.40	7ms
MD [19] (Stu.)	✓	7.78	7ms
Ours(Tea.)	-	7.66	0.12s
Ours(Stu.)		11.86	0.05s
Ours(Stu.)	✓	7.23	0.05s

Comparison with other distillation methods. To further demonstrate the effectiveness of the AMFD, we also compare other distillation methods in the field of multispectral pedestrian detection. The results are shown in Tab.VII. The MD [19] decreases the MR^{-2} of the student network by 1.62% after distillation, which indicates that the student network is good relative to the Knowledge Transfer Module proposed by the author. The MD method reduces the inference time (without post-processing treatments) by 36.3%. The DCRD [18] remains 3.42% higher than its DCRL teacher network in terms of MR^{-2} has a 26.8% reduction in the inference time. In contrast, AMFD can significantly improve the performance of a simple student network, even a little better than that of teacher networks.

Comparison with the state-of-the-art. To evaluate the superiority of our proposed method, we compare our method

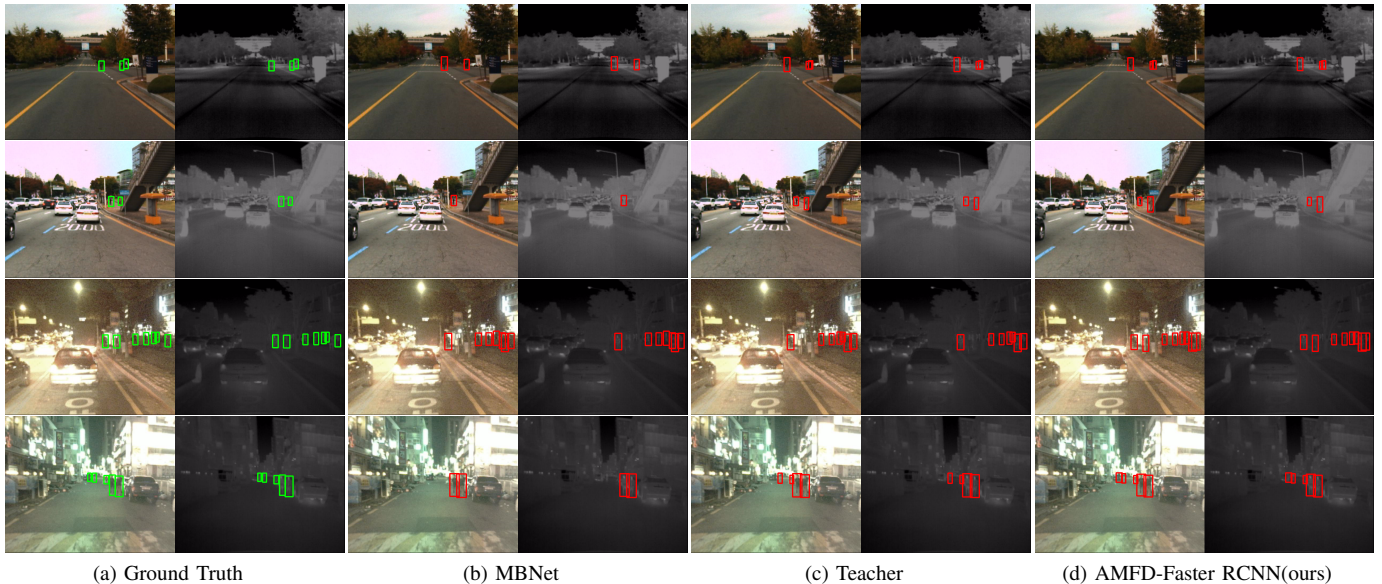


Fig. 9. Qualitative comparison of our (d) AMFD-Faster RCNN with (b) MBNet [24] and (c) the teacher network (ResNet50 × 2) on the KAIST [3] test set. The first two rows and the last two rows of images are daytime and nighttime results, respectively. Green and red boxes indicate the ground-truth bounding box and detector predictions, respectively.

with some existing state-of-the-art multispectral pedestrian detection methods on KAIST dataset trained by the improved annotation [35] namely IAF-RCNN [42], CIAN [43], AR-CNN [35], MBNet [24], BAANet [10], UFF+UCG [44], AANet [11]. We compare the MR^{-2} under three subsets: **All**, **Day** and **Night** and inference time with the state-of-the-art methods. As shown in Tab.IV, among these methods, AANet-Faster RCNN [11] has the best performance with achieving a log-average miss rate of 6.91% on the **All** set. Though our AMFD-Faster RCNN with a log-average miss rate of 7.23% and AMFD-RetinaNet with a log-average miss rate of 8.82% are slightly worse than AANet [11], the 0.05s and 0.04s inference time already far outperform all existing methods. Comparisons show that AMFD strikes a good balance between model performance and model compression and achieves excellent results in both aspects.

Qualitative comparison. Fig.9 displays the qualitative comparisons between our AMFD-Faster RCNN with (b) MBNet [24] and (c) the teacher network (ResNet50 × 2) on the KAIST [3] test set. The first two rows and the last two rows of images are day-time and night-time results, respectively. It can be observed that MBNet loses a few pedestrians in detection especially for small objects, whereas our AMFD-Faster RCNN trained by the teacher network can detect pedestrians in various illumination conditions. It is worth noting that sometimes our student networks can perform better than teacher networks. For example, in the third line, the student network detected a pedestrian that neither the teacher network nor MBNet detected. This confirms the fact that our distillation method indeed frees the student network from the constraints of the teacher network.

D. Distillation on LLVIP Dataset

Comparison with other distillation methods. Many excellent methods have been proposed on how to perform efficient distillation in object detection tasks. In this section, we will compare the distillation results of MGD [45], CWD [46], PKD [47] and our AMFD on the LLVIP dataset from the two-stream teacher network to the single-stream student network. We first obtain the experimental results of the state-of-the-art methods in the traditional distillation architecture that distill the fusion feature. Then we obtain experimental results using these distillation methods under our fusion distillation architecture. As shown in Tab.VIII, under the fusion distillation architecture, our AMFD can increase mAP by 2.7% which is better than other distillation methods. However, we found that not all distillation methods have better performance under the fusion distillation architecture, which suggests that the fusion distillation architecture and the MEA module are inseparable in our AMFD.

TABLE VIII
THE COMPARISON OF DISTILLATION RESULTS OF STATE-OF-THE-ART DISTILLATION METHODS FOR DETECTION ON LLVIP DATASET.

Methods	Backbone	mAP	AP ₅₀	AP ₇₅
Faster-RCNN (Teacher)	ResNet50 (×2)	59.4	96.9	66.8
Faster-RCNN (Student)	ResNet18 (×1)	55.6	93.6	60.4
<i>without fusion distillation architecture (distill fusion feature)</i>				
MGD [45]	ResNet18 (×1)	57.2(+1.6)	94.5	62.7
CWD [46]	ResNet18 (×1)	57.5 (+1.9)	95.3	63.6
PKD [47]	ResNet18 (×1)	57.6 (+2.0)	94.5	64.3
<i>with fusion distillation architecture</i>				
MGD [45]	ResNet18 (×1)	56.3(+0.7)	93.9	61.2
CWD [46]	ResNet18 (×1)	57.2 (+1.6)	95.3	63.0
PKD [47]	ResNet18 (×1)	57.7 (+2.1)	95.5	63.0
AFMD(ours)	ResNet18 (×1)	58.3 (+2.7)	95.2	64.9

Qualitative comparison. As shown in Fig.10, We select a daytime and a nighttime image to visualize the spatial feature attention of the networks, respectively. We can see that pedestrians are well segmented by blue areas (lower values) in the feature map of the teacher network in the second column. However, the student network based on the same fusion strategy in the third column shows more noise in the feature map in the daytime scenario. The student network obtained by our AMFD in the fourth column represents the pedestrian’s head with a blue region (low values) and the pedestrian’s body with an orange region (high values), which is completely different from the fusion strategy of the teacher network. This suggests that our AMFD can form a more robust and flexible fusion strategy independently from teacher networks, which better fits the structure of the student network than that of the teacher network.

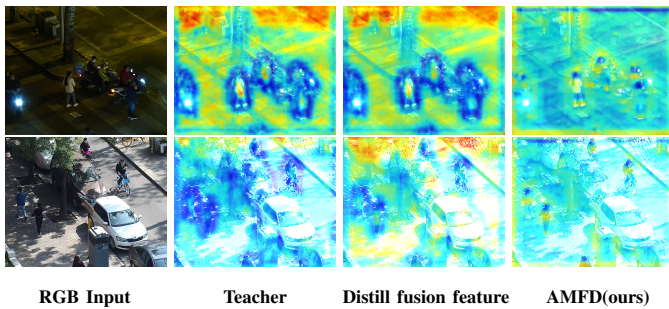


Fig. 10. Feature visualizations of fusion feature of the teacher network, the student network which distills the fusion feature of the teacher and the student obtained by our AMFD. It can be seen that the student network based on the same fusion strategy in the third column shows more noise in the feature map in the daytime, while our AMFD uses a completely different form of pedestrian feature representation from the teacher network.

E. Distillation on SMOD Dataset

Analysis of distillation results. In order to validate the effectiveness of our method on our SMOD dataset, we compared the distillation results using the traditional distillation architecture with the distillation results using the AMFD. The traditional distillation architecture distills only the fusion features of the teacher network with one single MEA module. In Tab.IX we can see that our AMFD improves the mAP of the student network by 3.5%, which is 0.6% more than the traditional distillation architecture that distills only fusion features. As for MR^{-2} , our distillation method also outperforms the traditional distillation architecture and obtains results that are on the same level as the teacher network. The above results

illustrate the effectiveness of our proposed fusion distillation architecture.

Comparison with other distillation methods. We perform a comparison with advanced distillation methods MGD [45], CWD [46] and PKD [47] in the previous Sec.V-D. In order to verify the flexibility of our distillation method, we perform distillation experiment using one stage detection network Retinanet [6]. From Tab.X, we can see that our AMFD can increase mAP by 4.0% which is better than other distillation methods in the one-stage detection network.

TABLE X
THE COMPARISON OF DISTILLATION RESULTS OF STATE-OF-THE-ART DISTILLATION METHODS FOR DETECTION ON SMOD DATASET.

Methods	Backbone	mAP	AP ₅₀	AP ₇₅
Retinanet (Tea.)	ResNet50 (×2)	65.1	91.8	77.1
Retinanet (Stu.)	ResNet18 (×1)	59.8	89.5	69.1
<i>without fusion distillation architecture (distill fusion feature)</i>				
PKD [47]	ResNet18 (×1)	62.1 (+2.3)	90.5	72.9
MGD [45]	ResNet18 (×1)	63.1 (+3.2)	90.5	73.5
CWD [46]	ResNet18 (×1)	63.6 (+3.8)	91.7	74.8
<i>with fusion distillation architecture</i>				
MGD [45]	ResNet18 (×1)	61.7 (+1.9)	89.9	72.2
PKD [47]	ResNet18 (×1)	61.9 (+2.1)	91.2	72.6
CWD [46]	ResNet18 (×1)	62.2 (+2.4)	91.4	73.0
AMFD(ours)	ResNet18 (×1)	63.8 (+4.0)	91.5	75.3

Effectiveness of the proposed MEA module. In the fusion distillation architecture, we use two MEA modules to force student networks to learn TIR and RGB features, respectively. In particular, we visualize the weights of the channels obtained in the MEA global feature extraction part (the $C \times 1 \times 1$ weights that we denote in Equation (3) by the symbol $\mathcal{W}(x)$). As shown in Fig.11, we can see that for different channels, there is a significant difference between the weights of the TIR MEA and the RGB MEA. This phenomenon of enhancement

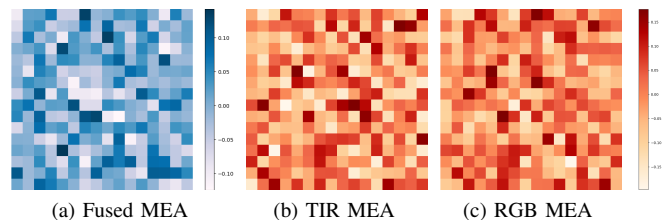


Fig. 11. Channel weights visualizations of the Fused MEA module in traditional distillation and TIR, RGB MEA modules in our AMFD. This shows that in our fusion distillation architecture, the two MEA modules can adaptively extract different useful information in TIR and RGB modalities.

TABLE IX
COMPARISON OF DISTILLATION RESULTS BETWEEN TRADITIONAL AND FUSION DISTILLATION ARCHITECTURES ON SMOD DATASET. THE "RGB", "TIR" AND "FUSION" DENOTE WHETHER DISTILL THE RGB, TIR AND FUSION FEATURE RESPECTIVELY.

Method	Distill			mAP	AP ₅₀	AP ₇₅	All	Day	Night
	RGB	TIR	Fusion						
Faster-RCNN (Teacher, 2×R50)	-	-	-	66.3	92.3	78.7	2.17	2.91	1.55
Faster-RCNN (Student, 1×R18)	-	-	-	60.6	88.6	71.3	3.33	4.55	2.34
Traditional Architecture(MEA×1)			✓	63.5(+2.9)	91.2	74.6	2.38(↓ 0.95)	3.34	1.46
AMFD (MEA×2,ours)	✓	✓		64.1(+3.5)	91.4	75.7	2.17(↓ 1.16)	3.05	1.44



Fig. 12. Qualitative comparison of our (d) student network distilled by AMFD with (b) the teacher network (ResNet50 \times 2) and (c) the student network (ResNet18 \times 1) without distillation on the SMOD test set. The first and second rows of the images are the daytime and nighttime results, respectively. Green and red boxes indicate the ground truth bounding box and detector predictions, respectively.

or weakness for different channels illustrates the effectiveness of our MEA module in fusion distillation architectures. In the traditional distillation architecture, we use only one MEA module to distill the fusion feature of teacher network. This generates only a single group of channel weights for the fusion features, which results in the missing useful latent information in both modalities.

Qualitative comparison. As shown in Fig12, we compare the student before and after distillation using AMFD and the teacher network. The first column of ground truth shows both visible and infrared images, and the rest of the images are visible pictures and spatial attention maps. From the detection results, it is clear that the student network before distillation is subject to false and missed detection. And the performance of our distilled student network is significantly improved and sometimes shows better performance than the teacher network. From the spatial attention maps, there is a large amount of noise in the student network before distillation compared to the teacher network. The distilled student network gets better detection results because our AMFD takes a different form of spatial attention representation.

VI. CONCLUSION

In this paper, we proposed an adaptive modal fusion distillation (AMFD) framework. This framework adopts the fusion distillation architecture, which can significantly improve the performance of student network. This architecture allows for a fusion strategy of the student network is independent from the teacher network. The modal extraction alignment (MEA) module extracts the original modal feature based on focal and global attention mechanisms. This distillation method can efficiently improve the performance of the student network, leading to efficient compression of the teacher network, which can substantially reduce the inference time for multispectral networks. Experiments show that the simple student network with faster inference speed can perform as well as the teacher network with AMFD. This makes it more feasible to deploy multispectral pedestrian detection capabilities in embedded devices in the future.

REFERENCES

[1] Z. Yang, J. Li, and H. Li, “Real-time pedestrian and vehicle detection for autonomous driving,” in *IEEE Intell. Vehicles Symp.* IEEE, 2018, pp. 179–184.

[2] M. Bilal, A. Khan, M. U. K. Khan, and C.-M. Kyung, “A low-complexity pedestrian detection framework for smart video surveillance systems,” *IEEE Trans. Circuits Syst. Video Technol.*, vol. 27, no. 10, pp. 2260–2273, 2016.

[3] S. Hwang, J. Park, N. Kim, Y. Choi, and I. So Kweon, “Multispectral pedestrian detection: Benchmark dataset and baseline,” in *Proc. IEEE Conf. Comput. Vis. Pattern Recognit.*, 2015, pp. 1037–1045.

[4] K. He, X. Zhang, S. Ren, and J. Sun, “Deep residual learning for image recognition,” in *Proc. IEEE Conf. Comput. Vis. Pattern Recognit.*, 2016, pp. 770–778.

[5] S. Ren, K. He, R. Girshick, and J. Sun, “Faster r-cnn: Towards real-time object detection with region proposal networks,” *IEEE Trans. Pattern Anal. Mach. Intell.*, vol. 39, no. 6, pp. 1137–1149, 2017.

[6] T.-Y. Lin, P. Goyal, R. Girshick, K. He, and P. Dollár, “Focal loss for dense object detection,” in *Proc. IEEE Int. Conf. Comput. Vis.*, 2017, pp. 2980–2988.

[7] D. Xu, W. Ouyang, E. Ricci, X. Wang, and N. Sebe, “Learning cross-modal deep representations for robust pedestrian detection,” in *Proc. IEEE Conf. Comput. Vis. Pattern Recognit.*, 2017, pp. 5363–5371.

[8] H. Zhang, E. Fromont, S. Lefèvre, and B. Avignon, “Guided attentive feature fusion for multispectral pedestrian detection,” in *Proc. IEEE/CVF Winter Conf. Appl. Comput. Vis.*, 2021, pp. 72–80.

[9] Y.-T. Chen, J. Shi, Z. Ye, C. Mertz, D. Ramanan, and S. Kong, “Multimodal object detection via probabilistic ensembling,” in *Proc. Eur. Conf. Comput. Vis.* Springer, 2022, pp. 139–158.

[10] X. Yang, Y. Qian, H. Zhu, C. Wang, and M. Yang, “Baanet: Learning bi-directional adaptive attention gates for multispectral pedestrian detection,” in *Proc. IEEE Int. Conf. Rob. Autom.* IEEE, 2022, pp. 2920–2926.

[11] N. Chen, J. Xie, J. Nie, J. Cao, Z. Shao, and Y. Pang, “Attentive alignment network for multispectral pedestrian detection,” in *Proc. ACM Int. Conf. Multimed.*, 2023, pp. 3787–3795.

[12] X. Zhang, X. Zhang, Z. Sheng, and H.-L. Shen, “Tfdet: Target-aware fusion for rgb-t pedestrian detection,” *arXiv preprint arXiv:2305.16580*, 2023.

[13] R. Li, J. Xiang, F. Sun, Y. Yuan, L. Yuan, and S. Gou, “Multiscale cross-modal homogeneity enhancement and confidence-aware fusion for multispectral pedestrian detection,” *IEEE Trans. Multimedia*, 2023.

[14] Q. Li, C. Zhang, Q. Hu, H. Fu, and P. Zhu, “Confidence-aware fusion using Dempster-Shafer theory for multispectral pedestrian detection,” *IEEE Trans. on Multimedia*, 2022.

[15] S. S. Kruthiventi, P. Sahay, and R. Biswal, “Low-light pedestrian detection from rgb images using multi-modal knowledge distillation,” in *Proc. IEEE Int. Conf. Image Process.* IEEE, 2017, pp. 4207–4211.

[16] Z. Luo, J.-T. Hsieh, L. Jiang, J. C. Niebles, and L. Fei-Fei, “Graph distillation for action detection with privileged modalities,” in *Proc. Eur. Conf. Comput. Vis.*, 2018, pp. 166–183.

[17] N. C. Garcia, P. Morerio, and V. Murino, “Learning with privileged information via adversarial discriminative modality distillation,” *IEEE Trans. Pattern Anal. Mach. Intell.*, vol. 42, no. 10, pp. 2581–2593, 2019.

[18] T. Liu, K.-M. Lam, R. Zhao, and G. Qiu, “Deep cross-modal representation learning and distillation for illumination-invariant pedestrian detection,” *IEEE Trans. Circuits Syst. Video Technol.*, vol. 32, no. 1, pp. 315–329, 2021.

[19] H. Zhang, E. Fromont, S. Lefèvre, and B. Avignon, “Low-cost multi-spectral scene analysis with modality distillation,” in *Proc. IEEE/CVF Winter Conf. Appl. Comput. Vis.*, 2022, pp. 803–812.

- [20] S. I. Mirzadeh, M. Farajtabar, A. Li, N. Levine, A. Matsukawa, and H. Ghasemzadeh, "Improved knowledge distillation via teacher assistant," in *Proc. AAAI Conf. Artif. Intell.*, vol. 34, no. 04, 2020, pp. 5191–5198.
- [21] M. Gao, Y. Wang, and L. Wan, "Residual error based knowledge distillation," *Neurocomputing*, vol. 433, pp. 154–161, 2021.
- [22] Y. Cao, J. Xu, S. Lin, F. Wei, and H. Hu, "Gcnet: Non-local networks meet squeeze-excitation networks and beyond," in *Proc. IEEE Int. Conf. Comput. Vis.*, 2019, pp. 1971–1980.
- [23] X. Jia, C. Zhu, M. Li, W. Tang, and W. Zhou, "Lvip: A visible-infrared paired dataset for low-light vision," in *Proc. IEEE Int. Conf. Comput. Vis.*, 2021, pp. 3496–3504.
- [24] K. Zhou, L. Chen, and X. Cao, "Improving multispectral pedestrian detection by addressing modality imbalance problems," in *Proc. Eur. Conf. Comput. Vis.* Springer, 2020, pp. 787–803.
- [25] C. Li, D. Song, R. Tong, and M. Tang, "Multispectral pedestrian detection via simultaneous detection and segmentation," *arXiv preprint arXiv:1808.04818*, 2018.
- [26] J. Xie, R. M. Anwer, H. Cholakkal, J. Nie, J. Cao, J. Laaksonen, and F. S. Khan, "Learning a dynamic cross-modal network for multispectral pedestrian detection," in *Proc. ACM Int. Conf. Multimed.*, 2022, pp. 4043–4052.
- [27] G. Hinton, O. Vinyals, and J. Dean, "Distilling the knowledge in a neural network," *arXiv preprint arXiv:1503.02531*, 2015.
- [28] R. Adriana, B. Nicolas, K. S. Ebrahimi, C. Antoine, G. Carlo, and B. Yoshua, "Fitnets: Hints for thin deep nets," *Proc. Int. Conf. Learn. Represent.*, vol. 2, no. 3, p. 1, 2015.
- [29] S. Zagoruyko and N. Komodakis, "Paying more attention to attention: Improving the performance of convolutional neural networks via attention transfer," *arXiv preprint arXiv:1612.03928*, 2016.
- [30] T. Wang, L. Yuan, X. Zhang, and J. Feng, "Distilling object detectors with fine-grained feature imitation," in *Proc. IEEE Conf. Comput. Vis. Pattern Recognit.*, 2019, pp. 4933–4942.
- [31] J. Guo, K. Han, Y. Wang, H. Wu, X. Chen, C. Xu, and C. Xu, "Distilling object detectors via decoupled features," in *Proc. IEEE Conf. Comput. Vis. Pattern Recognit.*, 2021, pp. 2154–2164.
- [32] A. González, Z. Fang, Y. Socarras, J. Serrat, D. Vázquez, J. Xu, and A. M. López, "Pedestrian detection at day/night time with visible and fir cameras: A comparison," *Sensors*, vol. 16, no. 6, p. 820, 2016.
- [33] J. Liu, X. Fan, Z. Huang, G. Wu, R. Liu, W. Zhong, and Z. Luo, "Target-aware dual adversarial learning and a multi-scenario multi-modality benchmark to fuse infrared and visible for object detection," in *Proc. IEEE Conf. Comput. Vis. Pattern Recognit.*, 2022, pp. 5802–5811.
- [34] T.-Y. Lin, P. Dollár, R. Girshick, K. He, B. Hariharan, and S. Belongie, "Feature pyramid networks for object detection," in *Proc. IEEE Conf. Comput. Vis. Pattern Recognit.*, 2017, pp. 2117–2125.
- [35] L. Zhang, X. Zhu, X. Chen, X. Yang, Z. Lei, and Z. Liu, "Weakly aligned cross-modal learning for multispectral pedestrian detection," in *Proc. IEEE Int. Conf. Comput. Vis.*, 2019, pp. 5127–5137.
- [36] J. Liu, S. Zhang, S. Wang, and D. N. Metaxas, "Multispectral deep neural networks for pedestrian detection," *arXiv preprint arXiv:1611.02644*, 2016.
- [37] T.-Y. Lin, M. Maire, S. Belongie, J. Hays, P. Perona, D. Ramanan, P. Dollár, and C. L. Zitnick, "Microsoft coco: Common objects in context," in *Proc. Eur. Conf. Comput. Vis.* Springer, 2014, pp. 740–755.
- [38] K. Chen, J. Wang, J. Pang, Y. Cao, Y. Xiong, X. Li, S. Sun, W. Feng, Z. Liu, J. Xu *et al.*, "Mmdetection: Open mmlab detection toolbox and benchmark," *arXiv preprint arXiv:1906.07155*, 2019.
- [39] A. Paszke, S. Gross, S. Chintala, G. Chanan, E. Yang, Z. DeVito, Z. Lin, A. Desmaison, L. Antiga, and A. Lerer, "Automatic differentiation in pytorch," 2017.
- [40] W.-Y. Lee, L. Jovanov, and W. Philips, "Cross-modality attention and multimodal fusion transformer for pedestrian detection," in *Proc. Eur. Conf. Comput. Vis.* Springer, 2022, pp. 608–623.
- [41] O. Russakovsky, J. Deng, H. Su, J. Krause, S. Satheesh, S. Ma, Z. Huang, A. Karpathy, A. Khosla, M. Bernstein *et al.*, "Imagenet large scale visual recognition challenge," *Int. J. Comput. Vision*, vol. 115, pp. 211–252, 2015.
- [42] C. Li, D. Song, R. Tong, and M. Tang, "Illumination-aware faster r-cnn for robust multispectral pedestrian detection," *Pattern Recogn.*, vol. 85, pp. 161–171, 2019.
- [43] L. Zhang, Z. Liu, S. Zhang, X. Yang, H. Qiao, K. Huang, and A. Husain, "Cross-modality interactive attention network for multispectral pedestrian detection," *Inf. Fusion*, vol. 50, pp. 20–29, 2019.
- [44] J. U. Kim, S. Park, and Y. M. Ro, "Uncertainty-guided cross-modal learning for robust multispectral pedestrian detection," *IEEE Trans. Circuits Syst. Video Technol.*, vol. 32, no. 3, pp. 1510–1523, 2021.

- [45] Z. Yang, Z. Li, M. Shao, D. Shi, Z. Yuan, and C. Yuan, "Masked generative distillation," in *Proc. Eur. Conf. Comput. Vis.* Springer, 2022, pp. 53–69.
- [46] C. Shu, Y. Liu, J. Gao, Z. Yan, and C. Shen, "Channel-wise knowledge distillation for dense prediction," in *Proc. IEEE Int. Conf. Comput. Vis.*, 2021, pp. 5311–5320.
- [47] W. Cao, Y. Zhang, J. Gao, A. Cheng, K. Cheng, and J. Cheng, "Pkd: General distillation framework for object detectors via pearson correlation coefficient," *Adv. neural inf. proces. syst.*, vol. 35, pp. 15 394–15 406, 2022.



Zizhao Chen received the B.S. degree in automation from Shanghai Jiao Tong University, Shanghai, China, in 2024. He is currently working toward the M.S. degree in Institute of Artificial Intelligence and Robotics of Xi'an Jiao Tong University.

His main research interests include computer vision, pattern recognition, machine learning, and their applications in intelligent transportation systems.



Ye qiang Qian received a Ph.D. degree in control science and engineering from Shanghai Jiao Tong University, Shanghai, China, in 2020. He is currently a Tenure Track Associate Professor in the Department of Automation at Shanghai Jiao Tong University, Shanghai, China.

His main research interests include computer vision, pattern recognition, machine learning, and their applications in intelligent transportation systems.



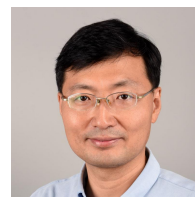
Xiaoxiao Yang received the B.S. degree in automation from Tongji University, Shanghai, China, in 2021. He is currently pursuing the M.S. degree in Shanghai Jiao Tong University, Shanghai, China.

His main research interests include computer vision, deep learning, and their applications in intelligent transportation systems.



Chunxiang Wang received his Ph.D. degree in mechanical engineering from the Harbin Institute of Technology, Harbin, China, in 1999.

She is currently an Associate Professor with the Department of Automation at Shanghai Jiao Tong University, Shanghai, China. Her research interests include robotic technology and electromechanical integration.



Ming Yang received Master and Ph.D. degrees from Tsinghua University, Beijing, China, in 1999 and 2003, respectively.

He is currently the Full Tenure Professor at Shanghai Jiao Tong University, the deputy director of the Innovation Center of Intelligent Connected Vehicles. He has been working in the field of intelligent vehicles for more than 20 years. He participated in several related research projects, such as the THMRV project (first intelligent vehicle in China), European CyberCars and CyberMove projects, CyberC3 project, CyberCars-2 project, ITER transfer cask project, AGV, etc.